Original Article

Magnetic resonance-based radiomics nomogram for predicting microsatellite instability status in endometrial cancer

Zijing Lin[1,2,3#], Ting Wang[2#], Haiming Li[2,3], Meiling Xiao[1], Xiaoliang Ma[1], Yajia Gu[2,3], Jinwei Qiang[1]

[1]Department of Radiology, Jinshan Hospital, Fudan University, Shanghai, China; [2]Department of Radiology, Fudan University Shanghai Cancer Center, Shanghai, China; [3]Department of Oncology, Shanghai Medical College, Fudan University, Shanghai, China

Contributions: (I) Conception and design: Z Lin, T Wang; (II) Administrative support: H Li, Y Gu, J Qiang; (III) Provision of study materials or patients: H Li, Y Gu, X Ma; (IV) Collection and assembly of data: Z Lin, T Wang, H Li, X Ma; (V) Data analysis and interpretation: Z Lin, T Wang, M Xiao; (VI) Manuscript writing: All authors; (VII) Final approval of manuscript: All authors.

[#]These authors contributed equally to this work.

Correspondence to: Jinwei Qiang. Department of Radiology, Jinshan Hospital, Fudan University, 1508 Longhang Road, Shanghai 201508, China. Email: dr.jinweiqiang@163.com; Yajia Gu. Department of Radiology, Shanghai Cancer Center; Department of Oncology, Shanghai Medical College, Fudan University, No. 270 Dongan Road, Shanghai 200032, China. Email: cjr.guyajia@vip.163.com.

Background: Microsatellite instability (MSI) status is an important indicator for screening patients with endometrial cancer (EC) who have potential Lynch syndrome (LS) and may benefit from immunotherapy. This study aimed to develop a magnetic resonance imaging (MRI)-based radiomics nomogram for the prediction of MSI status in EC.

Methods: A total of 296 patients with histopathologically diagnosed EC were enrolled, and their MSI status was determined using immunohistochemical (IHC) analysis. Patients were randomly divided into the training cohort (n=236) and the validation cohort (n=60) at a ratio of 8:2. To predict the MSI status in EC, the tumor radiomics features were extracted from T2-weighted images and contrast-enhanced T1-weighted images, which in turn were selected using one-way analysis of variance (ANOVA) and the least absolute shrinkage and selection operator (LASSO) algorithm to build the radiomics signature (radiomics score; radscore) model. Five clinicopathologic characteristics were used to construct a clinicopathologic model. Finally, the nomogram model combining radscore and clinicopathologic characteristics was constructed. The performance of the three models was evaluated using receiver operating characteristic (ROC), calibration, and decision curve analyses (DCA).

Results: Totals of 21 radiomics features and five clinicopathologic characteristics were selected to develop the radscore and clinicopathological models. The radscore and clinicopathologic models achieved an area under the curve (AUC) of 0.752 and 0.600, respectively, in the training cohort; and of 0.723 and 0.615, respectively, in the validation cohort. The radiomics nomogram model showed improved discrimination efficiency compared with the radscore and clinicopathologic models, with an AUC of 0.773 and 0.740 in the training and validation cohorts, respectively. The calibration curve analysis and DCA showed favorable calibration and clinical utility of the nomogram model.

Conclusions: The nomogram incorporating MRI-based radiomics features and clinicopathologic characteristics could be a potential tool for the prediction of MSI status in EC.

Keywords: Endometrial cancer (EC); microsatellite instability (MSI); magnetic resonance imaging (MRI); radiomics; nomogram

Submitted Mar 18, 2022. Accepted for publication Sep 05, 2022. Published online Oct 19, 2022.
doi: 10.21037/qims-22-255
View this article at: https://dx.doi.org/10.21037/qims-22-255

Introduction

Endometrial cancer (EC) is one of the most common malignancies of the female reproductive system, with an increasing incidence worldwide (1). In China, there were an estimated 69,000 new cases and 16,000 deaths in 2015, making uterine cancer the second most common gynecologic malignancy next to the cervical cancer (2). It is a heterogeneous disease with various molecular features, including microsatellite instability (MSI). By inactivating tumor suppressor genes, the mutations resulting from MSI can drive oncogenesis (3,4). Reports have shown that MSI is a common molecular alteration in different tumor types, among which EC has the highest prevalence, followed by colorectal cancer (CRC) (3,5).

Microsatellites are short repetitive nucleotide sequences in DNA which tend to cause errors during replication due to DNA polymerase slippage (6). The term MSI refers to the hypermutator phenotype that occurs in tumors with deficient DNA mismatch repair (MMR) (7). A significant proportion of Lynch syndrome (LS) caused by pathogenic germline mutations in MMR genes (8) shows MSI. Meanwhile, EC often occurs as sentinel cancer in women with LS (9). Therefore, testing of MSI status is important for the selection of treatment strategies and the prevention of secondary malignancies in patients with EC (10,11). In addition, studies have shown that MSI status has therapeutic implications, since patients with advanced-stage MSI cancers and metastastic MSI solid tumors might greatly benefit from immunotherapy (12,13). Since the approval of pembrolizumab for the treatment of unresectable or metastastic MSI solid tumors in 2017, the assessment of MSI status has become vital for all advanced cancers, including ECs (13). Currently, MSI status is mainly assessed in two ways: MSI testing and MMR assessment, both of which are highly concordant with each other and sensitive and specific (14). However, screening is expensive and not universal beyond tertiary centers (15). Hence, given the common use of magnetic resonance imaging (MRI) in patients with EC, developing a noninvasive and economical method to detect MSI/MMR status is of great importance for screening patients who might benefit from immunotherapy, and for improving the prognosis of these patients.

Radiomics is an emerging field which can measure associations between high-throughput information extracted from medical images and clinical outcomes to support personalized decision-making (16,17). Compared with conventional medical imaging, radiomics can expose disease characteristics that are invisible to the naked eye and has a great potential to capture important phenotype information and thus offer more valuable imaging biomarkers. Recently, radiomics has been widely applied in research of EC, such as the evaluation of risk stratification, lymph node metastasis (LNM), myometrial infiltration, and lymphovascular space invasion (LVSI) (18-20). Few studies have focused on the assessment of MSI status of EC. One study (21) demonstrated moderate prediction performance of MSI when using a CT-based radiomics model; however, pelvic CT is not the first choice for preoperative evaluation of gynecologic patients (21,22). As a first-choice imaging technique with superior tissue resolution, MRI has been shown to optimize the preoperative evaluation of patients with EC.

Therefore, this study aimed to develop a radiomics nomogram based on MRI and clinicopathologic information to predict MSI status in patients with EC. We present the following article in accordance with the TRIPOD reporting checklist (available at https://qims.amegroups.com/article/view/10.21037/qims-22-255/rc).

Methods

Study population

The study was conducted in accordance with the Declaration of Helsinki (as revised in 2013). This retrospective study was approved by the institutional review board of Fudan University Shanghai Cancer Center (FUSCC), and individual consent for this retrospective analysis was waived. We reviewed 412 patients with histopathologically diagnosed EC who had undergone pelvic MRI examination within 2 weeks before surgery in FUSCC between January 2017 and December 2020. The exclusion criteria were as follows: (I) no immunohistochemistry (IHC) for MMR proteins (MSH2, MSH6, MLH1, and PMS2) was available (n=68); (II) a lack of definable lesions on MRI (n=42); (III) errors when opening images using MITK software to segmented tumors (n=4); or (IV) patients had already received neoadjuvant chemotherapy (NACT) (n=2). Finally, a total of 296 patients with EC and IHC-supported MSI/MMR status were included in this study (*Figure 1*). Patients were randomly divided into the training cohort (n=236) and the validation cohort (n=60) according to a ratio of 8:2.

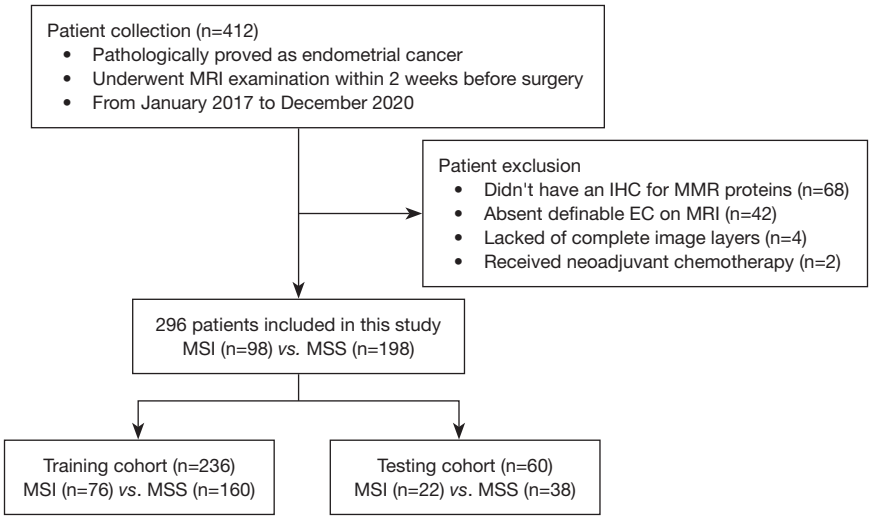

Figure 1 Data flow diagram of the study population. IHC, immunohistochemistry; MMR, DNA mismatch repair; EC, endometrial cancer; MRI, magnetic resonance imaging; MSI, microsatellite instability; MSS, microsatellite stability.

Clinicopathologic characteristics

The following clinicopathologic data were recorded: patient age, menopausal status, reproductive history, history of hypertension and diabetes mellitus, obesity, tumor histopathologic type, grade, lower uterine segment involvement (LUSI), presence of myometrial invasion (MI), LVSI, LNM, International Federation of Gynecology and Obstetrics (FIGO) stage, and serum carbohydrate antigen (CA)125 and CA199 levels. Obesity was defined as a body mass index (BMI) ≥28 kg/m^2 (23), and the tumor was staged according to the FIGO cancer report 2018 (24).

MSI status assessment

The MSI status was determined via IHC staining of four MMR proteins (MLH1, MSH2, PMS2, and MSH6). Tumors with loss of expression of at least one of the four MMR proteins were classified as MSI or deficient mismatch repair (dMMR). In contrast, tumors with expression of all four MMR proteins were classified as microsatellite stability (MSS) or proficient mismatch repair (pMMR) (22).

MRI acquisition

All MRI were performed with a 1.5T or 3.0T MR scanner (Signa HDxt or Pioneer, GE, Milwaukee, WI, USA; Skyra, Prisma or Verio, Siemens, Erlangen, Germany; uMR 588, United Imaging, Shanghai, China). Patients lay supinely and breathed freely. The T2-weighted images (T2WI) and contrast-enhanced T1-weighted images (CE-T1WI) were archived for subsequent analysis. The parameters were as follows: for T2WI sequence, slice thickness: 4.0–6.0 mm, matrix: 256/512×256/512, repetition time: 2,015–4,200 ms, and echo time: 72.1–138.2 ms; and for CE-T1WI sequence, slice thickness: 3.0–6.0 mm, matrix: 256/512×256/512, repetition time: 3.51–6.77 ms, and echo time: 1.29–3.21 ms. The contrast agent (Magnevist, Bayer Schering, Berlin, German) was intravenously administrated at a dose of 0.2 mL/kg body weight and an injection rate of 2–3 mL/s.

Tumor segmentation and radiomics feature extraction

Blinded to the patients' clinical and pathologic information, the tumors were manually delineated slice-by-slice on sagittal T2WI and CE-T1WI to obtain volume of interest (VOI) by a junior radiologist (reader 1 with 3 years of experience in gynecologic imaging) using Medical Imaging Interaction Toolkit (MITK) software (version 2016.11.3; http://www.mitk.org/). Examples of tumor segmentation are shown in Figure S1 in a supplementary online appendix.

Each image was normalized by centering it at the mean with standard deviation. Meanwhile, voxel sizes were resampled into 1 mm^3 by applying a B-spline curve interpolation algorithm. For each MRI sequence, quantitative radiomics features were extracted from VOIs using the open-access Python package, PyRadiomics v3.0.1 (http://www.radiomics.io/pyradiomics.html). The

extracted features were divided into six categories: 18 first-order features, 24 gray level co-occurrence matrix (GLCM) features, 16 gray level size zone matrix (GLSZM) features, 16 gray level run length matrix (GLRLM) features, 5 neighboring gray tone difference matrix (NGTDM) features, and 14 gray level dependence matrix (GLDM) features. All these feature classes were extracted from the original image and eight derived images applying eight image filters: wavelet, Laplacian of Gaussian (LoG, σ=1.0, 2.0, 3.0, 4.0), square, square root, logarithm, exponential, gradient, and local binary pattern (LBP) in 3D. In addition, 14 3D shape features were only extracted from the original image. Ultimately, a total of 1,967 radiomics features were extracted for each VOI from T2WI and CE-T1WI images.

The MRI images of 30 patients were randomly chosen to evaluate inter- and intra-observer agreement of radiomics features. To assess intra-observer reproducibility, reader 1 repeatedly segmented the VOI on T2WI and CE-T1WI after two weeks. To assess inter-observer reproducibility, the second radiologist (reader 2, with 8 years of experience in gynecologic imaging) also independently performed VOI delineation, and radiomics features were extracted in an identical manner. The intraclass and interclass correlation coefficients (ICCs) were computed to evaluate the reproducibility of radiomics features. Features with ICCs lower than 0.75 indicating poor agreement were removed (25).

Feature selection and radiomics signature construction

For T2WI- and CE-T1WI-based radiomics features, one-way analysis of variance (ANOVA) was performed to eliminate the features that showed no significant differences between MSI and MSS tumors. All of the remaining features were included in the feature pool. After normalizing these features using z-score normalization, the least absolute shrinkage and selection operator (LASSO) algorithm was used to remove the redundant features and identify the optimal features using 10-fold cross-validation. The radiomics signature (Rradscore) was calculated for each patient using a linear combination of the selected features, which were weighted by their respective regression coefficients. Moreover, the Wilcoxon rank sum test was employed to evaluate the significant differences in the selected radiomics features with non-zero coefficients for predicting MSI tumors.

Five clinicopathologic features including age, grade, LUSI, and diabetes mellitus and reproductive history, which have been previously reported to be associated with MSI/MMR status and LS-associated EC (26-29), were selected to build the clinicopathologic model.

Development and evaluation of prediction model

Three models, namely the radscore model, clinicopathologic model, and nomogram model combining the radiomics signature and clinicopathologic factors were developed using logistic regression in the training cohort. The optimal model selection was determined based on the Akaike information criterion (AIC).

The performance of the established models was evaluated based on three criteria. First, discrimination performance was assessed using receiver operating characteristic (ROC) curve analysis and quantified using the area under the curve (AUC) with a corresponding 95% confidence interval (CI), accuracy, sensitivity, and specificity. Net reclassification index (NRI) and total integrated discrimination index (IDI) were used to evaluate the additional benefit of the proposed model. Second, calibration performance was assessed through calibration curves measuring the agreement between the predicted and actual probability. Third, clinical application of the models was assessed using decision curve analysis (DCA), which quantified the net benefit for the interval of threshold probabilities. The flow chart of the study is displayed in *Figure 2*.

Statistical analysis

Mann-Whitney U, chi-square, or Fisher exact tests were used, as appropriate, to analyze significant differences of clinicopathologic features in the training and validation cohorts. Radiomics feature extraction was performed with Python programming language version 3.8 (Python Software Foundation, Wilmington, DE, USA). Statistical analysis of clinicopathologic features, radiomics feature selection, model building, and evaluation were conducted using R software version 3.5.2 (The R Foundation for Statistical Computing, Vienna, Austria). A P value <0.05 was considered significant for all two-sided tests.

Results

Patient profiles

The 296 patients included 98 patients with MSI and 198 patients with MSS. The clinicopathologic features of MSI and MSS tumors in the training and validation cohorts

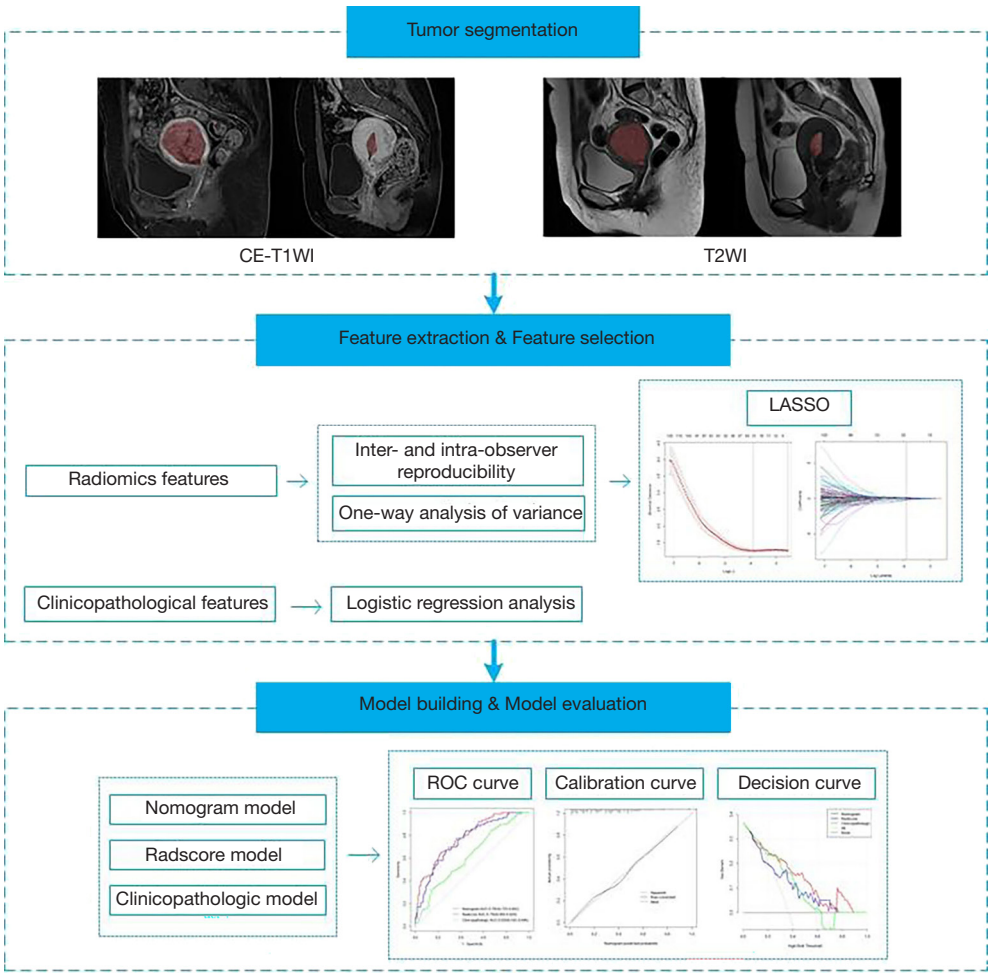

Figure 2 Flow chart of the study including tumor segmentation, feature extraction, feature selection, model building, and model evaluation. CE-T1WI, contrast-enhanced T1-weighted image; T2WI, T2-weighted image; LASSO, least absolute shrinkage and selection operator; ROC, receiver operating characteristic.

are shown in *Table 1*. There were no significant differences in clinicopathologic features between patients with different MSI status in either cohort, except for grade in the validation cohort (P=0.024).

Feature selection and radscore building

Of the T2WI- and CE-T1WI-based radiomics features, 1,759 and 1,802 features were considered stable, respectively (inter- and intraobserver ICCs ≥0.75); 333 and 44 significant features for MSI were retained, respectively, after ANOVA; and 21 most valuable radiomics features were selected using LASSO in the training cohort (*Figure 3*). The radscore of each patient was calculated using the 21 radiomics features with non-zero coefficients (Table S1). More detailed information is included in the supplementary online appendix. Moreover, the radscores were significantly different between MSI and MSS tumors in the training cohort (P<0.0001) and in the validation cohort (P<0.01) (*Figure 4*).

Development and evaluation of the nomogram

The selected five clinicopathologic features (age, grade, LUSI, diabetes mellitus and reproductive history) and 21 radiomics features were used to construct a clinicopathologic model and a radscore model, respectively. The nomogram model (*Figure 5*) was further constructed integrating clinicopathologic and radiomics factors.

The ROC curves of the three models in both the training and validation cohorts are presented in *Figure 6*. The AUC

Table 1 Clinicopathologic characteristics of patients with MSI and MSS tumors in the training and validation cohorts

Clinicopathologic characteristics	Subgroups	Training cohort			Validation cohort		
		MSI (n=76)	MSS (n=160)	P value	MSI (n=22)	MSS (n=38)	P value
Age (years)	<60	60 (78.9)	110 (68.8)	0.103	16 (72.7)	29 (76.3)	0.757
	≥60	16 (21.1)	50 (31.3)		6 (27.3)	9 (23.7)	
Histopathologic type	EEC	68 (89.5)	148 (92.5)	0.435	22 (100.0)	35 (92.1)	0.292
	Non-EEC	8 (10.5)	12 (7.5)		0 (0.0)	3 (7.9)	
Grade	1	28 (36.8)	63 (39.4)	0.920	3 (13.6)	15 (39.5)	0.024
	2	31 (40.8)	64 (40.0)		17 (77.3)	15 (39.5)	
	3	17 (22.4)	33 (20.6)		2 (9.1)	8 (21.1)	
MI	<1/2	51 (67.1)	107 (66.9)	0.942	15 (68.2)	24 (63.2)	0.837
	≥1/2	16 (21.1)	36 (22.5)		6 (27.3)	10 (26.3)	
	None	9 (11.8)	17 (10.6)		1 (4.5)	4 (10.5)	
LVSI	(+)	13 (17.1)	26 (16.3)	0.869	7 (31.8)	6 (15.8)	0.197
	(–)	63 (82.9)	134 (83.8)		15 (68.2)	32 (84.2)	
LNM	(+)	4 (5.3)	11 (6.9)	0.635	1 (4.5)	2 (5.3)	1.000
	(–)	72 (94.7)	149 (93.1)		21 (95.5)	36 (94.7)	
FIGO stage	I	65 (85.5)	130 (81.3)	0.396	19 (86.4)	29 (76.3)	0.784
	II	4 (5.3)	17 (10.6)		2 (9.1)	6 (15.8)	
	III–IV	7 (9.2)	13 (8.1)		1 (4.5)	3 (7.9)	
LUSI	(+)	15 (19.7)	25 (15.6)	0.431	4 (18.2)	4 (10.5)	0.449
	(–)	61 (80.3)	135 (84.4)		18 (81.8)	34 (89.5)	
Menopausal status	Post-	39 (51.3)	96 (60.0)	0.208	14 (63.6)	22 (57.9)	0.662
	Pre-	37 (48.7)	64 (40.0)		8 (36.4)	16 (42.1)	
Reproductive history	Yes	74 (97.4)	145 (90.6)	0.061	21 (95.5)	35 (92.1)	1.000
	No	2 (2.6)	15 (9.4)		1 (4.5)	3 (7.9)	
Hypertension	(+)	22 (28.9)	55 (34.4)	0.406	7 (31.8)	15 (39.5)	0.591
	(–)	54 (71.1)	105 (65.6)		15 (68.2)	23 (60.5)	
Diabetes mellitus	(+)	5 (6.6)	21 (13.1)	0.133	1 (4.5)	6 (15.8)	0.246
	(–)	71 (93.4)	139 (86.9)		21 (95.5)	32 (84.2)	
Obesity	(+)	13 (17.1)	32 (20.0)	0.597	3 (13.6)	7 (18.4)	0.732
	(–)	63 (82.9)	128 (80.0)		19 (86.4)	31 (81.6)	
CA125 (U/mL)		27.95±36.79	30.47±56.69	0.911	23.83±15.49	24.22±18.21	0.555
CA199 (U/mL)		29.06±73.72	29.54±84.34	0.123	17.57±14.89	19.82±17.34	0.679

Continuous variables are shown as mean ± standard deviation. Categorical variables are shown as number of patients with percentages in parentheses. MSI, microsatellite instability; MSS, microsatellite stability; EEC, endometrial endometrioid carcinoma; MI, myometrial invasion; LVSI, lymphovascular space invasion; LNM, lymph node metastasis; FIGO, International Federation of Gynecology and Obstetrics; LUSI, lower uterine segment involvement; CA125, carbohydrate antigen 125; CA199, carbohydrate antigen 199.

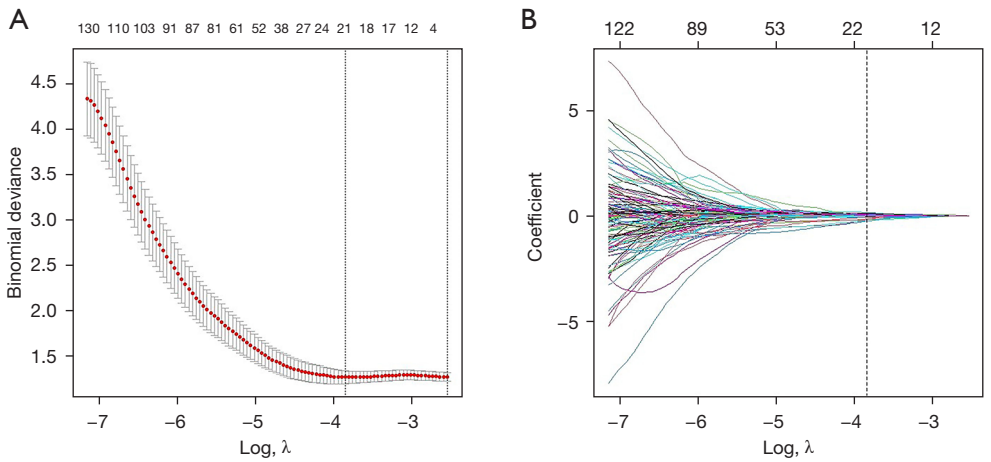

Figure 3 Radiomics feature selection using the LASSO algorithm. (A) Tuning parameter (λ) selection in the LASSO model via 10-fold cross-validation based on minimum criterion. The optimal λ value of 0.0214 with log (λ) =−3.85 was selected. (B) A LASSO coefficient profile plot of the 377 radiomics features. The vertical line indicates the coefficient size of each resulting feature and the corresponding selected log (λ). LASSO, least absolute shrinkage and selection operator.

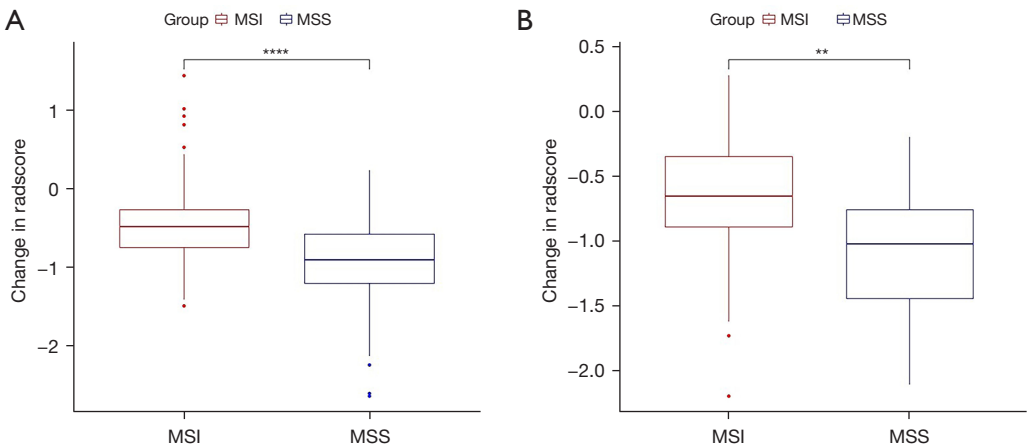

Figure 4 Boxplots show the difference in the radscore between the MSI and MSS tumors in the training (A) and validation cohorts (B). **, P<0.01; ****, P<0.0001. MSI, microsatellite instability; MSS, microsatellite stability.

for predicting MSI in the clinicopathologic, radscore, and radiomics nomogram models were 0.600 (95% CI: 0.526 to 0.674), 0.752 (95% CI: 0.688 to 0.817), and 0.773 (95% CI: 0.712 to 0.834) in the training cohort, respectively; and 0.615 (95% CI: 0.467 to 0.763), 0.723 (95% CI: 0.576 to 0.869), and 0.740 (95% CI: 0.596 to 0.885) in the validation cohort, respectively. The corresponding accuracy, sensitivity, and specificity values are listed in *Table 2*. The nomogram model significantly improved risk reclassification for MSI status compared with the clinicopathologic model, with a categorical NRI of 22.4% (95% CI: 7.1% to 37.7%) and IDI of 17.3% (95% CI: 11.9% to 22.7%) in the training cohort, and a categorical NRI of 46.6% (95% CI: 17.5% to 75.8%) and IDI of 17.0% (95% CI: 6.7% to 27.3%) in the validation cohort (all P<0.05).

The calibration curve of the nomogram demonstrated good consistency between prediction and observation in the training and validation cohorts (*Figure 7*). The DCA for the three models in the validation cohort is presented in *Figure 8*. The decision curve showed that the nomogram model could add more net benefit than 'none' or 'all' treatment within a range from 0.03 to 0.05 and

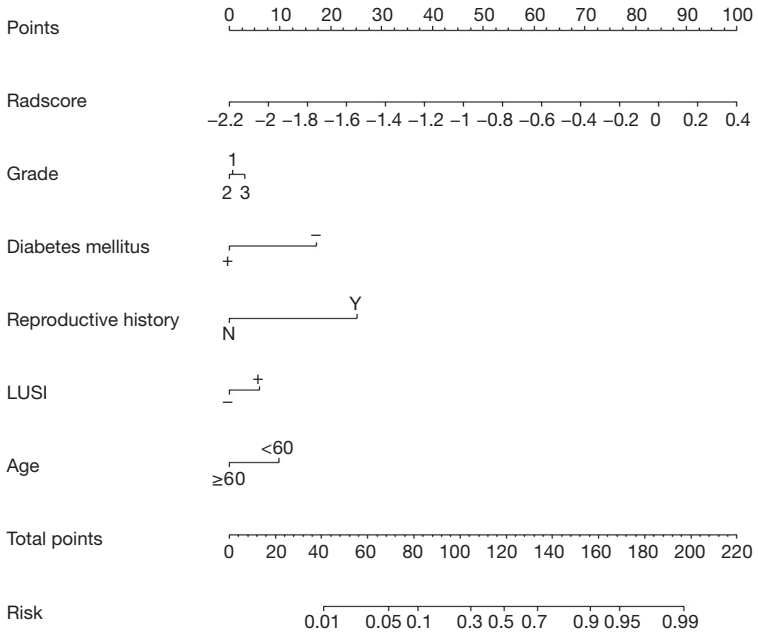

Figure 5 Development of radiomics nomogram based on five selected clinicopathologic features and radscore. LUSI, lower uterine segment involvement.

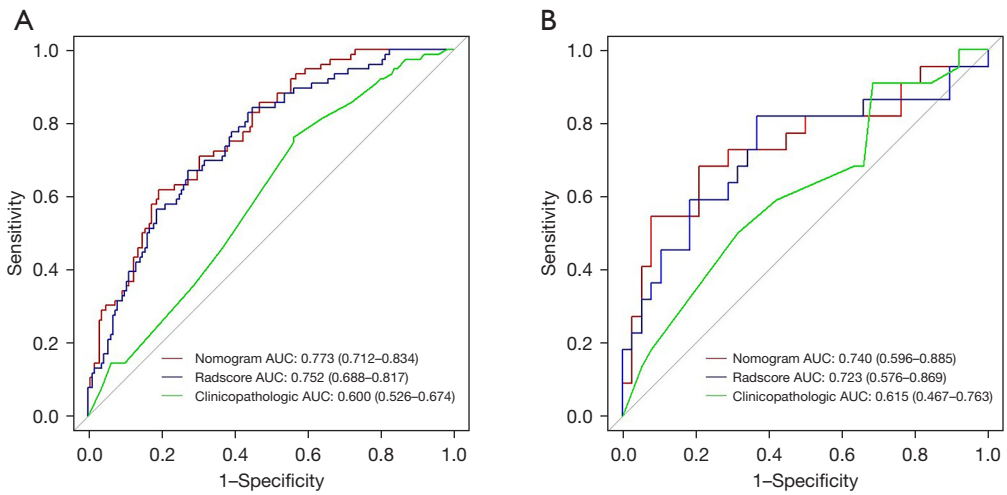

Figure 6 The ROC curves of clinicopathologic, radscore, and nomogram models in the training (A) and validation (B) cohorts. AUC, area under the curve; ROC, receiver operating characteristic.

0.12 to 0.90 of threshold probability, while the radscore and clinicopathologic models could add more net benefit within a range of 0.22 to 0.76, 0.04 to 0.16, and 0.20 to 0.63, respectively. The nomogram presented better clinical usefulness compared to the radscore and clinicopathologic models.

Discussion

To the best of our knowledge, very few studies have focused on the evaluation of MSI status of EC by using a radiomics-based method. In this study, we developed a radiomics nomogram to assess MSI status based on preoperative pelvic MRI images in patients with EC. Our results indicated that

Table 2 Prediction performance of clinicopathologic, radscore, and nomogram models

Model	Training cohort				Validation cohort			
	AUC (95% CI)	ACU	SEN	SPE	AUC (95% CI)	ACU	SEN	SPE
Clinicopathologic	0.600 (0.526–0.674)	0.542	0.763	0.438	0.615 (0.467–0.763)	0.467	0.682	0.342
Radscore	0.752 (0.688–0.817)	0.708	0.671	0.725	0.723 (0.576–0.869)	0.683	0.455	0.816
Nomogram	0.773 (0.712–0.834)	0.746	0.618	0.806	0.740 (0.596–0.885)	0.767	0.500	0.921

AUC, the area under the curve; CI, confidence interval; ACU, accuracy; SEN, sensitivity; SPE, specificity.

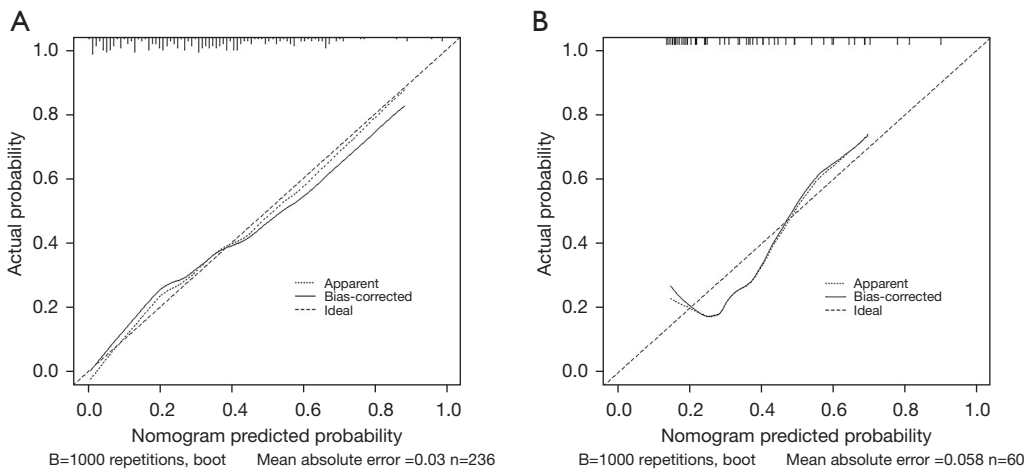

Figure 7 Calibration curves of the nomogram in the training (A) and validation (B) cohorts. The diagonal line represents the perfect match between nomogram-predicted and actual probability. The solid line represents bias-corrected estimated results of the nomogram employing 1,000 bootstrap sampling.

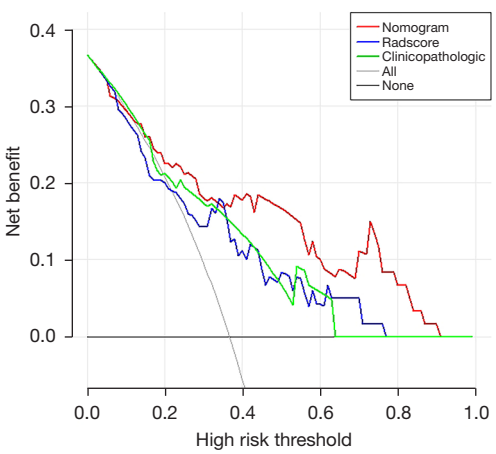

Figure 8 Decision curve analysis of the clinicopathologic, radscore, and nomogram models in the validation cohort. The clinicopathologic, radscore, and nomogram models add more net benefit than 'none' or 'all' treatment within a range of 0.04 to 0.16 and 0.20 to 0.63, 0.22 to 0.76, 0.03 to 0.05, and 0.12 to 0.90, respectively.

the developed nomogram combining radiomics features and clinicopathologic factors showed favorable discrimination efficiency for predicting MSI status of EC and demonstrated good fitness and clinical usefulness.

MSI is common in different malignancies, especially in EC and CRC (30). A previous study reported a prevalence of MSI of 26–33% in EC (31). In our study, approximately 33% of EC had MSI, and this prevalence was similar to that of other studies (5,32). Assessing MSI status is important to screen for LS-related EC and to identify patients who might benefit from immunotherapy. However, MSI assessment using polymerase chain reaction (PCR) or IHC is not widely used in many basic medical institutions (33). Hence, the need remains to develop new biomarkers to help identify MSI status of EC.

High-throughput information extracted from medical images with radiomics methods commonly comprises histogram features, shape features, and texture features, which could help capture tumor heterogeneity to provide clinical decision support (34). Several studies have

demonstrated that radiomics features could be used as valuable biomarkers to help identify MSI status in CRC and EC. Studies by Cao, Fan, and Golia Pernicka *et al.* (33,35,36) achieved a favorable predictive performance for MSI status in CRC by combining CT based-radiomics features with clinical signatures. Moreover, Zhang *et al.* (37) and Li *et al.* (38) developed MRI-based radiomics models and achieved excellent predictive efficacy for MSI in rectal cancer. Regarding EC, Veeraraghavan *et al.* (21) adopted machine learning by integrating radiomics features extracted from contrast-enhanced CT images and clinical factors and achieved moderate accuracy in distinguishing MMR-deficient and mutational burden-high (TMB-H) ECs. However, the inherent limitation of CT images to display tumors hinders CT-based radiomics clinical application. In contrast, given the advantages of excellent soft tissue resolution, multiparameter imaging, and nonionizing radiation, MRI based-radiomics models may, therefore, provide more valuable information (22,39).

In this study, we built three predictive models to predict MSI status of EC: a clinicopathologic model based on clinicopathologic characteristics, a radscore model based on radiomics features extracted from MRI images, and a nomogram combining radscore and clinicopathologic characteristics. We chose five relevant factors to develop the clinicopathologic model and demonstrated its less than satisfactory performance in both cohorts. The results could possibly be explained by our sample, which differed from those in studies undertaken in other countries and showed no significant differences in terms of these clinicopathologic features. Our results are consistent with Zhang *et al.*'s study (37) on rectal cancer and indicate that clinical information alone is insufficient to identify MSI status. A total of 21 radiomics features, including 16 features from T2WI and 5 features from CE-T1WI, were selected to build the radscore model. Among the selected features, the majority were extracted from the derived images. Furthermore, the radiomics nomogram, which incorporated radiomics features and clinicopathologic characteristics, achieved a higher discriminative performance than the radscore and clinicopathologic models. The reclassification measures of discrimination suggested that the nomogram model significantly improved the identification of MSI compared with the clinicopathologic model. These findings suggest that MRI-based radiomics features may offer additional biological information beyond clinicopathologic characteristics and have independent value in the prediction of MSI status in EC (40,41). Compared with Wang *et al.*'s (42) study based on quantitative shape features of the tumor, our nomogram showed better performance in predicting MSI status in EC. However, our nomogram model seemed to have lower predictive performance than the similar MRI-radiomics model of CRC. This is probably due to the less obvious heterogeneity in EC with different MSI status than in CRC (43). Moreover, MSI is tumor type-specific and impacts on gene expression and phenotype (44,45), which may account for the varying predictive performance in different tumor types. The DCA showed that our nomogram had greater net benefit than radscore or clinicopathologic characteristics models in the threshold probability of 0.03 to 0.05 and 0.12 to 0.90 in the assessment of MSI status in EC, and, therefore, demonstrated promising clinical utility. Even though the discriminative efficiency of our nomogram was only moderate, its favorable calibration performance and clinical utility indicated its clinical value.

Our study had several limitations. First, this was a retrospective study carried out in a single center, making selection bias inevitable. Moreover, the sample size was relatively small. Therefore, the results of the study need to be further validated by data from multicenter studies involving larger samples. Second, IHC was used to evaluate MSI status. Although IHC for MMR proteins assessment is a reliable and cost-effective technique for analysis of MSI status, PCR is still considered the gold standard for assessing MSI status. The disagreement between these two testing methods ranged from 2% to 8% according to different studies (8,46) and may have impacted our results. Third, due to incomplete data, diffusion-weighted imaging (DWI), a valuable sequence for EC subtyping, grading, and staging, was not used to develop the radiomics nomogram. Fourth, manual region of interest (ROI) segmentation was time-consuming and might have generated unavoidable observer bias (47). Consequently, deep learning-based image segmentation is recommended in the future.

In summary, we developed a radiomics nomogram incorporating MRI-based radiomics features and clinicopathologic characteristics to identify MSI status in EC. This nomogram could be a potential tool for screening LS, preventing second malignancies, and selecting patients who might benefit from immunotherapy.

Acknowledgments

Funding: This work was supported by the Shanghai Health and Family Planning Commission Youth Fund Project (No.

20194Y0489), the Shanghai Municipal Health Commission (Nos. 2020YJZK0209 and ZK2019B01), and the National Natural Science Foundations of China (Nos. 81901704 and 81971579).

Footnote

Reporting Checklist: The authors have completed the TRIPOD reporting checklist. Available at https://qims.amegroups.com/article/view/10.21037/qims-22-255/rc

Conflicts of Interest: All authors have completed the ICMJE uniform disclosure form (available at https://qims.amegroups.com/article/view/10.21037/qims-22-255/coif). The authors have no conflicts of interest to declare.

Ethical Statement: The authors are accountable for all aspects of the work in ensuring that questions related to the accuracy or integrity of any part of the work are appropriately investigated and resolved. The study was conducted in accordance with the Declaration of Helsinki (as revised in 2013). The study was approved by the institutional review board of Fudan University Shanghai Cancer Center, and individual consent for this retrospective analysis was waived.

References

1. Lu KH, Broaddus RR. Endometrial Cancer. N Engl J Med 2020;383:2053-64.
2. Zhang S, Sun K, Zheng R, Zeng H, Wang S, Chen R, Wei W, He J. Cancer incidence and mortality in China, 2015. Journal of the National Cancer Center 2021;1:2-11.
3. Hause RJ, Pritchard CC, Shendure J, Salipante SJ. Classification and characterization of microsatellite instability across 18 cancer types. Nat Med 2016;22:1342-50.
4. Di Tucci C, Capone C, Galati G, Iacobelli V, Schiavi MC, Di Donato V, Muzii L, Panici PB. Immunotherapy in endometrial cancer: new scenarios on the horizon. J Gynecol Oncol 2019;30:e46.
5. McGrail DJ, Garnett J, Yin J, Dai H, Shih DJH, Lam TNA, et al. Proteome Instability Is a Therapeutic Vulnerability in Mismatch Repair-Deficient Cancer. Cancer Cell 2020;37:371-386.e12.
6. Cortes-Ciriano I, Lee S, Park WY, Kim TM, Park PJ. A molecular portrait of microsatellite instability across multiple cancers. Nat Commun 2017;8:15180.
7. Baretti M, Le DT. DNA mismatch repair in cancer. Pharmacol Ther 2018;189:45-62.
8. Stelloo E, Jansen AML, Osse EM, Nout RA, Creutzberg CL, Ruano D, Church DN, Morreau H, Smit VTHBM, van Wezel T, Bosse T. Practical guidance for mismatch repair-deficiency testing in endometrial cancer. Ann Oncol 2017;28:96-102.
9. Lu KH, Dinh M, Kohlmann W, Watson P, Green J, Syngal S, Bandipalliam P, Chen LM, Allen B, Conrad P, Terdiman J, Sun C, Daniels M, Burke T, Gershenson DM, Lynch H, Lynch P, Broaddus RR. Gynecologic cancer as a "sentinel cancer" for women with hereditary nonpolyposis colorectal cancer syndrome. Obstet Gynecol 2005;105:569-74.
10. Garg K, Leitao MM Jr, Kauff ND, Hansen J, Kosarin K, Shia J, Soslow RA. Selection of endometrial carcinomas for DNA mismatch repair protein immunohistochemistry using patient age and tumor morphology enhances detection of mismatch repair abnormalities. Am J Surg Pathol 2009;33:925-33.
11. Hampel H, Frankel W, Panescu J, Lockman J, Sotamaa K, Fix D, et al. Screening for Lynch syndrome (hereditary nonpolyposis colorectal cancer) among endometrial cancer patients. Cancer Res 2006;66:7810-7.
12. Sobecki-Rausch J, Barroilhet L. Anti-programmed Death-1 Immunotherapy for Endometrial Cancer with Microsatellite Instability-High Tumors. Curr Treat Options Oncol 2019;20:83.
13. Silveira AB, Bidard FC, Kasperek A, Melaabi S, Tanguy ML, Rodrigues M, Bataillon G, Cabel L, Buecher B, Pierga JY, Proudhon C, Stern MH. High-Accuracy Determination of Microsatellite Instability Compatible with Liquid Biopsies. Clin Chem 2020;66:606-13.
14. Kurnit KC, Westin SN, Coleman RL. Microsatellite instability in endometrial cancer: New purpose for an old test. Cancer 2019;125:2154-63.
15. Eriksson J, Amonkar M, Al-Jassar G, Lambert J, Malmenäs M, Chase M, Sun L, Kollmar L, Vichnin M. Mismatch Repair/Microsatellite Instability Testing Practices among US Physicians Treating Patients with Advanced/Metastatic

Colorectal Cancer. J Clin Med 2019;8:558.
16. Lambin P, Leijenaar RTH, Deist TM, Peerlings J, de Jong EEC, van Timmeren J, Sanduleanu S, Larue RTHM, Even AJG, Jochems A, van Wijk Y, Woodruff H, van Soest J, Lustberg T, Roelofs E, van Elmpt W, Dekker A, Mottaghy FM, Wildberger JE, Walsh S. Radiomics: the bridge between medical imaging and personalized medicine. Nat Rev Clin Oncol 2017;14:749-62.
17. Lambin P, Rios-Velazquez E, Leijenaar R, Carvalho S, van Stiphout RG, Granton P, Zegers CM, Gillies R, Boellard R, Dekker A, Aerts HJ. Radiomics: extracting more information from medical images using advanced feature analysis. Eur J Cancer 2012;48:441-6.
18. Manganaro L, Nicolino GM, Dolciami M, Martorana F, Stathis A, Colombo I, Rizzo S. Radiomics in cervical and endometrial cancer. Br J Radiol 2021;94:20201314.
19. Yan BC, Li Y, Ma FH, Zhang GF, Feng F, Sun MH, Lin GW, Qiang JW. Radiologists with MRI-based radiomics aids to predict the pelvic lymph node metastasis in endometrial cancer: a multicenter study. Eur Radiol 2021;31:411-22.
20. Yan BC, Li Y, Ma FH, Feng F, Sun MH, Lin GW, Zhang GF, Qiang JW. Preoperative Assessment for High-Risk Endometrial Cancer by Developing an MRI- and Clinical-Based Radiomics Nomogram: A Multicenter Study. J Magn Reson Imaging 2020;52:1872-82.
21. Veeraraghavan H, Friedman CF, DeLair DF, Ninčević J, Himoto Y, Bruni SG, et al. Machine learning-based prediction of microsatellite instability and high tumor mutation burden from contrast-enhanced computed tomography in endometrial cancers. Sci Rep 2020;10:17769.
22. Reinhold C, Ueno Y, Akin EA, Bhosale PR, Dudiak KM, Jhingran A, Kang SK, Kilcoyne A, Lakhman Y, Nicola R, Pandharipande PV, Paspulati R, Shinagare AB, Small W Jr, Vargas HA, Whitcomb BP, Glanc P. ACR Appropriateness Criteria® Pretreatment Evaluation and Follow-Up of Endometrial Cancer. J Am Coll Radiol 2020;17:S472-86.
23. Hu L, Huang X, You C, Li J, Hong K, Li P, Wu Y, Wu Q, Wang Z, Gao R, Bao H, Cheng X. Prevalence of overweight, obesity, abdominal obesity and obesity-related risk factors in southern China. PLoS One 2017;12:e0183934.
24. Amant F, Mirza MR, Koskas M, Creutzberg CL. Cancer of the corpus uteri. Int J Gynaecol Obstet 2018;143 Suppl 2:37-50.
25. Xue C, Yuan J, Lo GG, Chang ATY, Poon DMC, Wong OL, Zhou Y, Chu WCW. Radiomics feature reliability assessed by intraclass correlation coefficient: a systematic review. Quant Imaging Med Surg 2021;11:4431-60.
26. McMeekin DS, Tritchler DL, Cohn DE, Mutch DG, Lankes HA, Geller MA, Powell MA, Backes FJ, Landrum LM, Zaino R, Broaddus RD, Ramirez N, Gao F, Ali S, Darcy KM, Pearl ML, DiSilvestro PA, Lele SB, Goodfellow PJ. Clinicopathologic Significance of Mismatch Repair Defects in Endometrial Cancer: An NRG Oncology/Gynecologic Oncology Group Study. J Clin Oncol 2016;34:3062-8.
27. Grzankowski KS, Shimizu DM, Kimata C, Black M, Terada KY. Clinical and pathologic features of young endometrial cancer patients with loss of mismatch repair expression. Gynecol Oncol 2012;126:408-12.
28. Staff S, Aaltonen M, Huhtala H, Pylvänäinen K, Mecklin JP, Mäenpää J. Endometrial cancer risk factors among Lynch syndrome women: a retrospective cohort study. Br J Cancer 2016;115:375-81.
29. Zhao S, Chen L, Zang Y, Liu W, Liu S, Teng F, Xue F, Wang Y. Endometrial cancer in Lynch syndrome. Int J Cancer 2022;150:7-17.
30. Yang G, Zheng RY, Jin ZS. Correlations between microsatellite instability and the biological behaviour of tumours. J Cancer Res Clin Oncol 2019;145:2891-9.
31. Hempelmann JA, Lockwood CM, Konnick EQ, Schweizer MT, Antonarakis ES, Lotan TL, Montgomery B, Nelson PS, Klemfuss N, Salipante SJ, Pritchard CC. Microsatellite instability in prostate cancer by PCR or next-generation sequencing. J Immunother Cancer 2018;6:29.
32. Kandoth C, Schultz N, Cherniack AD, Akbani R, Liu Y, Shen H, Robertson AG, Pashtan I, Shen R, Benz CC, Yau C, Laird PW, Ding L, Zhang W, Mills GB, Kucherlapati R, Mardis ER, Levine DA. Integrated genomic characterization of endometrial carcinoma. Nature 2013;497:67-73.
33. Cao Y, Zhang G, Zhang J, Yang Y, Ren J, Yan X, Wang Z, Zhao Z, Huang X, Bao H, Zhou J. Predicting Microsatellite Instability Status in Colorectal Cancer Based on Triphasic Enhanced Computed Tomography Radiomics Signatures: A Multicenter Study. Front Oncol 2021;11:687771.
34. Luo Y, Mei D, Gong J, Zuo M, Guo X. Multiparametric MRI-Based Radiomics Nomogram for Predicting Lymphovascular Space Invasion in Endometrial Carcinoma. J Magn Reson Imaging 2020;52:1257-62.
35. Fan S, Li X, Cui X, Zheng L, Ren X, Ma W, Ye Z. Computed Tomography-Based Radiomic Features Could Potentially Predict Microsatellite Instability Status in

Stage II Colorectal Cancer: A Preliminary Study. Acad Radiol 2019;26:1633-40.
36. Golia Pernicka JS, Gagniere J, Chakraborty J, Yamashita R, Nardo L, Creasy JM, Petkovska I, Do RRK, Bates DDB, Paroder V, Gonen M, Weiser MR, Simpson AL, Gollub MJ. Radiomics-based prediction of microsatellite instability in colorectal cancer at initial computed tomography evaluation. Abdom Radiol (NY) 2019;44:3755-63.
37. Zhang W, Huang Z, Zhao J, He D, Li M, Yin H, Tian S, Zhang H, Song B. Development and validation of magnetic resonance imaging-based radiomics models for preoperative prediction of microsatellite instability in rectal cancer. Ann Transl Med 2021;9:134.
38. Li Z, Dai H, Liu Y, Pan F, Yang Y, Zhang M. Radiomics Analysis of Multi-Sequence MR Images For Predicting Microsatellite Instability Status Preoperatively in Rectal Cancer. Front Oncol 2021;11:697497.
39. Huang Z, Zhang W, He D, Cui X, Tian S, Yin H, Song B. Development and validation of a radiomics model based on T2WI images for preoperative prediction of microsatellite instability status in rectal cancer: Study Protocol Clinical Trial (SPIRIT Compliant). Medicine (Baltimore) 2020;99:e19428.
40. Pei Q, Yi X, Chen C, Pang P, Fu Y, Lei G, Chen C, Tan F, Gong G, Li Q, Zai H, Chen BT. Pre-treatment CT-based radiomics nomogram for predicting microsatellite instability status in colorectal cancer. Eur Radiol 2022;32:714-24.
41. Zhou Y, He L, Huang Y, Chen S, Wu P, Ye W, Liu Z, Liang C. CT-based radiomics signature: a potential biomarker for preoperative prediction of early recurrence in hepatocellular carcinoma. Abdom Radiol (NY) 2017;42:1695-704.
42. Wang H, Xu Z, Zhang H, Huang J, Peng H, Zhang Y, Liang C, Zhao K, Liu Z. The value of magnetic resonance imaging-based tumor shape features for assessing microsatellite instability status in endometrial cancer. Quant Imaging Med Surg 2022;12:4402-13.
43. Alba AC, Agoritsas T, Walsh M, Hanna S, Iorio A, Devereaux PJ, McGinn T, Guyatt G. Discrimination and Calibration of Clinical Prediction Models: Users' Guides to the Medical Literature. JAMA 2017;318:1377-84.
44. Gutman DA, Cooper LA, Hwang SN, Holder CA, Gao J, Aurora TD, et al. MR imaging predictors of molecular profile and survival: multi-institutional study of the TCGA glioblastoma data set. Radiology 2013;267:560-9.
45. Kim TM, Laird PW, Park PJ. The landscape of microsatellite instability in colorectal and endometrial cancer genomes. Cell 2013;155:858-68.
46. McConechy MK, Talhouk A, Li-Chang HH, Leung S, Huntsman DG, Gilks CB, McAlpine JN. Detection of DNA mismatch repair (MMR) deficiencies by immunohistochemistry can effectively diagnose the microsatellite instability (MSI) phenotype in endometrial carcinomas. Gynecol Oncol 2015;137:306-10.
47. van Timmeren JE, Cester D, Tanadini-Lang S, Alkadhi H, Baessler B. Radiomics in medical imaging-"how-to" guide and critical reflection. Insights Imaging 2020;11:91.

Cite this article as: Lin Z, Wang T, Li H, Xiao M, Ma X, Gu Y, Qiang J. Magnetic resonance-based radiomics nomogram for predicting microsatellite instability status in endometrial cancer. Quant Imaging Med Surg 2023;13(1):108-120. doi: 10.21037/qims-22-255

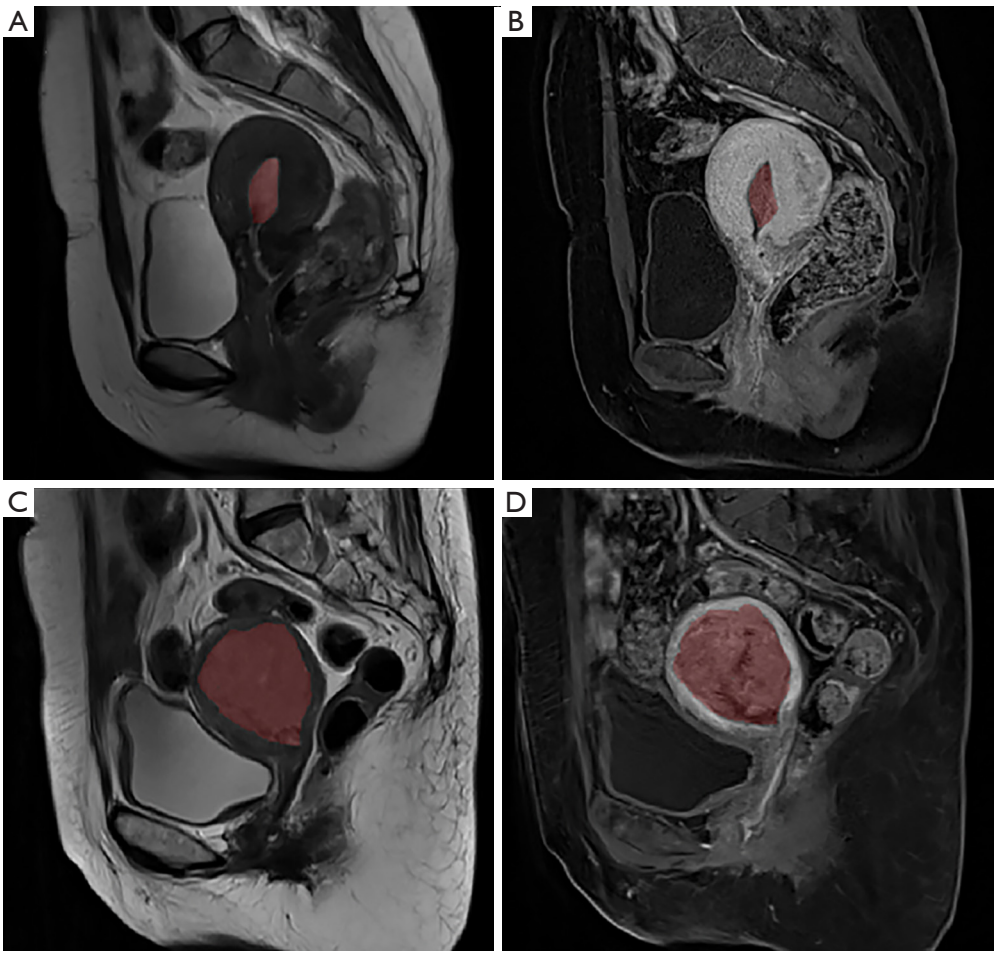

Figure S1 Examples of tumor segmentation. The tumors without myometrial invasion (A,B) and the tumors with deep myometrial invasion (C,D) were manually delineated on sagittal T2WI and CE-T1WI, respectively.

https://dx.doi.org/10.21037/qims-22-255

Table S1 Radscore calculation based on twenty-one selected features and the corresponding coefficients (intercept: –0.79839647)

Radiomics Features	Sequences	Coefficients
Original_glszm_GrayLevelNonUniformityNormalized	T2WI	–0.18022699
Log-sigma-2-0-mm-3D_firstorder_Median	T2WI	0.15777111
Wavelet-LLH_firstorder_90Percentile	T2WI	0.10232227
Wavelet-HHL_gldm_LargeDependenceHighGrayLevelEmphasis	T2WI	–0.24352681
Wavelet-LLL_firstorder_Median	T2WI	–0.01439181
Square_ngtdm_Contrast	T2WI	–0.07703857
Logarithm_firstorder_Mean	T2WI	–0.15783955
Logarithm_firstorder_Skewness	T2WI	0.02622695
Logarithm_glcm_ClusterShade	T2WI	0.03675137
Logarithm_gldm_LargeDependenceLowGrayLevelEmphasis	T2WI	0.09734627
Exponential_glcm_Idmn	T2WI	0.10942421
Gradient_firstorder_Uniformity	T2WI	0.08956594
Gradient_glrlm_ShortRunEmphasis	T2WI	–0.02669108
Lbp-3D-m1_glszm_GrayLevelVariance	T2WI	–0.25541521
Lbp-3D-m2_glcm_Idmn	T2WI	–0.01626632
Lbp-3D-k_firstorder_10Percentile	T2WI	0.02845274
Wavelet-HLH_glcm_MCC	CE-T1WI	–0.1836688
Square_gldm_LargeDependenceHighGrayLevelEmphasis	CE-T1WI	0.11834663
Squareroot_glrlm_GrayLevelNonUniformityNormalized	CE-T1WI	0.05317308
Squareroot_ngtdm_Contrast	CE-T1WI	–0.04020497
Lbp-3D-k_glrlm_ShortRunEmphasis	CE-T1WI	–0.07003751

https://dx.doi.org/10.21037/qims-22-255